Applied Catalysis B: Environmental 129 (2013) 1–12

Contents lists available at SciVerse ScienceDirect

Applied Catalysis B: Environmental

journal homepage: www.elsevier.com/locate/apcatb

Continuous-flow photocatalytic treatment of pharmaceutical micropollutants: Activity, inhibition, and deactivation of TiO_2 photocatalysts in wastewater effluent

Sean Carbonaro, Matthew N. Sugihara, Timothy J. Strathmann *

Department of Civil and Environmental Engineering and Center of Advanced Materials for the Purification of Water with Systems, University of Illinois at Urbana-Champaign, Newmark Civil Engineering Laboratory, MC-250, Urbana, IL 61801, USA

ARTICLE INFO

Article history:
Received 14 May 2012
Received in revised form 2 September 2012
Accepted 11 September 2012
Available online 19 September 2012

Keywords:
Wastewater treatment
Water reuse
Emerging contaminant
Photocatalyst
Thin film

ABSTRACT

Titanium dioxide (TiO_2) photocatalysts have been shown to be effective at degrading a wide range of organic micropollutants during short-term batch experiments conducted under ideal laboratory solution conditions (e.g., deionized water). However, little research has been performed regarding longer-term photocatalyst performance in more complex matrices representative of contaminated water sources (e.g., wastewater effluent, groundwater). Here, a benchtop continuous-flow reactor was developed for the purpose of studying the activity, inhibition, and deactivation of immobilized TiO_2 photocatalysts during water treatment applications. As a demonstration, degradation of four pharmaceutical micropollutants (iopromide, acetaminophen, sulfamethoxazole, and carbamazepine) was monitored in both a pH-buffered electrolyte solution and a biologically treated wastewater effluent (WWE) to study the effects of non-target constituents enriched in the latter matrix. Reactor performance was shown to be stable over 7 d when treating micropollutants in buffered electrolyte, with 7-d averaged k_{obs} values (acetaminophen = $0.97 \pm 0.10\ h^{-1}$; carbamazepine = $0.50 \pm 0.04\ h^{-1}$; iopromide = $0.49 \pm 0.03\ h^{-1}$; sulfamethoxazole = $0.79 \pm 0.06\ h^{-1}$) agreeing closely with measurements from short-term circulating batch reactions. When reactor influent was switched to WWE, treatment efficiencies decreased to varying degrees (acetaminophen = 40% decrease; carbamazepine = 60%; iopromide = 78%; sulfamethoxazole = 54%). A large fraction of the catalyst activity was recovered upon switching back to the buffered electrolyte influent after 4 d, suggesting that much of the observed decrease resulted from reversible inhibition by non-target constituents (e.g., scavenging of photocatalyst-generated $^{\bullet}OH$). However, there was also a portion of the decrease in activity that was not recovered, indicating WWE constituents also contributed to photocatalyst deactivation (acetaminophen = 6% deactivation; carbamazepine = 24%; iopromide = 16%; sulfamethoxazole = 25%). Experiments conducted using pretreated WWE and synthetic WWE mimic solutions indicated that both effluent organic matter and inorganic constituents in WWE contributed to the observed photocatalyst inhibition/deactivation. Analysis of immobilized TiO_2 thin films after 4 d of continuous treatment of the WWE matrix indicated minor deterioration of the porous film and formation of surface precipitates enriched in Al and Ca. Results demonstrated the marked influence of non-target constituents present in complex matrices on long-term photocatalyst activity and highlighted the need for further study of this important issue to advance the development of practical photocatalytic water treatment technologies.

1. Introduction

Although therapeutic use of pharmaceuticals has improved the quality of human life, concerns have also been raised about the fate of excreted drugs in the environment because many of these chemicals are recalcitrant to conventional wastewater treatment processes [1]. As a result, many pharmaceuticals have been detected as micropollutants in water supplies that receive inputs from wastewater treatment plants [2]. Although concentrations of these micropollutants in wastewater effluents are very low, usually ng/L to μg/L, concerns have been raised because little is known about the effects of chronic exposure to mixtures of these chemicals on sensitive aquatic organisms [3,4]. Human health concerns have also been raised, particularly in areas that have instituted recycled potable water programs (e.g., California, Arizona, and Florida), where potential exists for accumulation of persistent micropollutants as well as biologically active metabolites and degradates [4].

* Corresponding author. Tel.: +1 217 244 4679.
E-mail address: strthmnn@illinois.edu (T.J. Strathmann).

0926-3373/$ – see front matter © 2012 Elsevier B.V. All rights reserved.
http://dx.doi.org/10.1016/j.apcatb.2012.09.014

Concerns about the occurrence chemically diverse micropollutants have increased interest in the development of advanced treatment technologies capable of eliminating a wide spectrum of micropollutants. Advanced oxidation processes (AOPs) are promising treatment options [5,6]. Collectively, AOPs generate hydroxyl radical (•OH) which reacts non-selectively with most organic compounds at near diffusion-limited rates (e.g., k_2 values from 10^8 to $10^{10}\,M^{-1}\,s^{-1}$ at 25 °C [7]). For some highly recalcitrant contaminants, like iodinated X-ray contrast media, AOPs and high pressure membrane processes (e.g., reverse osmosis, nanofiltration) are the only effective treatment options [8–10].

Titanium dioxide (TiO_2) photocatalysis is a promising AOP that has demonstrated ability to degrade many micropollutants [11–13]. Irradiation of TiO_2 with ultraviolet (UV) light exceeding the semiconductor bandgap energy (E_g = 3.10 eV and 3.23 eV for rutile and anatase, respectively, corresponding to λ < 400 and 384 nm, respectively [14]) excites electrons from a filled valence band to an empty conduction band, creating electron-hole pairs. The valence band holes (h_{vb}^+) can initiate oxidative pathways (e.g., reacting with adsorbed H_2O to produce •OH), while conduction band electrons (e_{cb}^-) can react with adsorbed O_2 or other electron-accepting species, including some contaminants [15]. Advantages of TiO_2 photocatalytic treatment processes include the material's low cost and resistance to photocorrosion and chemical corrosion [16], and the potential use of solar irradiation [17]. Many current research efforts are aimed at modifying TiO_2 materials to expand their active range into visible regions of the solar spectrum (λ > 400 nm) [18].

Although a large body of literature has demonstrated that UV-TiO_2 photocatalysis is effective at transforming organic pollutants, the vast majority of studies have been conducted under idealized conditions using experimental systems that do not permit easy translation of results to more practical engineered treatment operations. Most experimental studies have been conducted in batch systems where suspensions of TiO_2 nanoparticles are irradiated [12,19–21], whereas in engineered treatment processes the catalysts will likely need to be immobilized on fixed support materials and contaminated water will be treated in a continuous-flow configuration. Most experimental studies have also focused on elucidation of detailed reaction kinetics and pathways for individual contaminants, and thus experiments were conducted using micropollutant concentrations (e.g., >1 mg/L) that are far greater than those measured in real water matrices (e.g., ng/L–μg/L), and target micropollutants are studied in the absence of non-target constituents that are typically present in natural water matrices at orders-of-magnitude higher concentration (e.g., natural organic matter, carbonate species and other major ions) [11,22]. Some studies have attempted to address these issues by studying photocatalytic treatment of micropollutants in natural water matrices or laboratory waters amended with important non-target constituents [12,23–27]; however, practical application of findings from these efforts is often limited because studies were conducted under artificial conditions where the target micropollutant concentration actually exceeded that of the non-target constituents, which poorly represents practical field conditions where non-target constituents constitute the majority of dissolved solids and organic matter and will act to scavenge a major fraction of reactive species generated by photocatalysts. Finally, batch experimental systems are inappropriate for studying the long-term activity of catalysts during real treatment operations where catalysts will be continuously exposed to a fresh influent stream of water that may contain low levels of substances that accumulate on catalyst surfaces over time leading to irreversible deactivation. Instead, continuous-flow experimental setups at varying scales are needed to examine these factors.

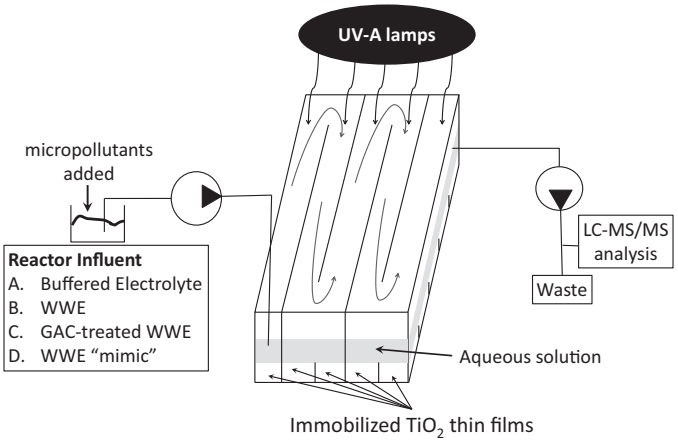

Fig. 1. Schematic of continuous-flow reactor and list of influent feed solutions examined in study.

To begin addressing some of these critical issues, here we describe the development of a laboratory benchtop continuous-flow photocatalyst reactor system that can be used to study catalyst activity, stability, inhibition and deactivation during continuous treatment of target micropollutants in both laboratory solution and natural water matrices relevant to the water treatment industry. Commercial TiO_2 nanoparticles were immobilized as thin films on glass supports (microscope slides) placed in a serpentine plug flow reactor and irradiated by commercial UV-A light sources (Fig. 1). While the reactor is not intended to replicate all the complexity of actual field-scale engineered processes, the laboratory-scale reactor enables preliminary investigation of factors that will be critical to the success of larger scale treatment processes (e.g., catalyst stability, inhibition, deactivation, and potential regeneration of deactivated catalysts). Immobilization of catalysts on microscope slides also facilitates analysis of the effects of treatment operations and matrix exposure on catalyst properties. In this contribution, we first established the stability and reproducibility of reactor performance through long-term (e.g., 1 week) continuous-flow experiments where a mixture of four pharmaceutical micropollutants (Fig. 2) is treated in a pH-buffered electrolyte solution. The performance of the reactor using a tertiary treated wastewater effluent (WWE) matrix was also examined as a model natural water matrix because of the interest in applying photocatalysis as an advanced treatment option for micropollutants that are recalcitrant to biological wastewater treatment processes. Individual micropollutants were selected for study as model compounds because of their expected recalcitrance to other wastewater treatment processes [1] and their documented transformation by TiO_2 photocatalysis [12,19,28].

2. Materials and methods

2.1. Supplies

All chemicals were reagent grade and were used as received from Sigma–Aldrich–Fluka or Fisher, unless otherwise indicated. Iopromide was provided as a gift from Schering AG (Berlin, Germany). Nanophase TiO_2 (primary particle size of 30 nm) composed of a mixture of anatase and rutile phases (Type P25, 50 $m^2\,g^{-1}$) was provided by Degussa [29]. Granular activated carbon (GAC; Filtrasorb 820) was obtained from Calgon Carbon Corporation. WWE was obtained from the outfall of the Urbana-Champaign Sanitary District (UCSD) Northeast Wastewater Treatment Facility. Prior to use, WWE was filtered sequentially with 10 μm and 1 μm membrane filters (Polygard-CR 10 μm

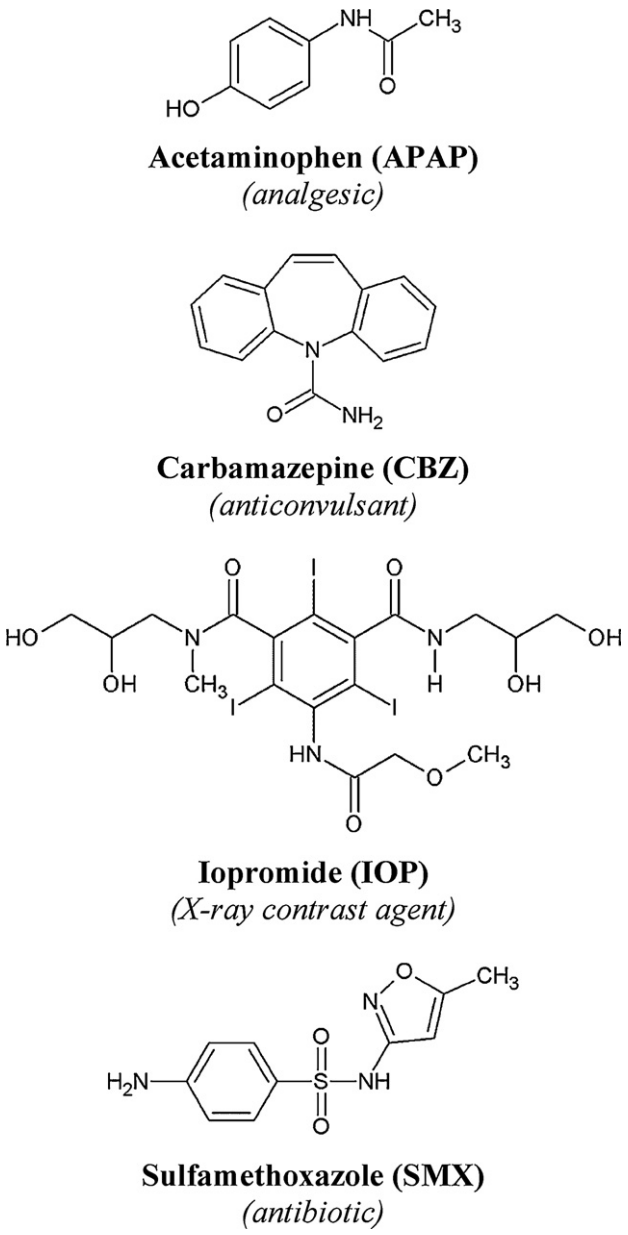

Fig. 2. Micropollutants used in study.

and Lifegard 1 μm, Millipore) and stored under darkness at 4 °C. Deionized water (DI; Barnstead NANOpure systems; >18 MΩ cm resistivity) was used to prepare all other solutions.

2.2. Immobilized TiO_2 thin films

Immobilized porous thin films of TiO_2 were prepared using a procedure modified from that described by Balasubramanian et al. [30]. Thirty grams per liter of TiO_2 nanoparticles (Degussa P25) was mixed into a TiO_2 sol–gel containing 0.42 M titanium isopropoxide (TTIP), 1.68 M diethanolamine, and 0.84 M water in isopropanol. Glass microscope slides (Fig. 3A; 75 mm × 25 mm × 1 mm; Thermo Scientific Gold Seal) were used as a substrate for depositing the thin films. An automated dipcoating apparatus was designed to hold five glass slides vertically and lift slides out of the sol gel mixture at a uniform rate of 20 cm/min. The coated slides were then placed on a rack and dried at room temperature for 24 h before heat treating in a programmable furnace. Heat treatment consisted of heating slides at 3 °C/min to 100 °C, holding for 1 h, then increasing at 3 °C/min to 600 °C, again holding for 1 h before cooling to ambient temperature. Three dip coating/heat treatment cycles were used because preliminary tests indicated no further improvement in photocatalytic activity with application of additional coatings.

2.3. Continuous-flow reactor

The activity of immobilized photocatalyst thin films was studied in a serpentine-pattern plug flow reactor (Fig. 1). The reactor was designed with five channels, each the width of 1 standard microscope slide (25 mm) and length of 5 slides (375 mm), for a total of 25 film-coated slides placed along the entire reactor flow path. Five 15 W 18 in. long UV-A lamps with spectrum centered at ~365 nm (manufactured by General Electric) were suspended and centered over each of the five channels (12 cm between lamp and film-coated slides). Inlet flow rate was controlled using a Masterflex L/S digital standard drive peristaltic pump, and reactor volume was controlled by placing weirs of varying height at the end of the plug flow reactor. For this study, a mean flow rate of 2.7 mL/min and weir height of 0.62 cm were used, resulting in a reactor volume of 325 mL, a theoretical hydraulic residence time of 120 min, and a Reynold's number of 5. The design residence time was selected to achieve between 50 and 90% degradation of the target micropollutants in a laboratory-prepared buffered electrolyte matrix (9 mM NaCl + 1 mM $NaHCO_3$) based upon preliminary test measurements of the immobilized photocatalyst activity measured under rapid circulating batch conditions. Designing experiments based upon this range of micropollutant degradation permitted better quantification of matrix effects than if design was based upon a higher level of treatment where changes in catalyst activity would be more difficult to quantify.

2.4. Reactor and catalyst characterization

Tracer studies were conducted using perchlorate, a photocatalytically inert species, to determine flow patterns. A pulse addition of $NaClO_4$ (5 mL of 5 mg/L) was introduced to the reactor influent, and then samples were periodically collected for analysis at a point directly before the outlet weir to monitor tracer breakthrough. Collected samples were filtered (0.22 μm cellulose acetate) and analyzed by ion chromatography (IC).

Potassium ferrioxalate actinometry [31] was used to quantify UVA flux incident on the reactor. UVA lamps were allowed to warm up for >1 h prior to measurement. Three solutions were prepared separately immediately before measurement: 87.5 mL of 0.3 M $Fe_2(SO_4)_3$, 87.5 mL of 1.8 M potassium oxalate ($K_2C_2O_4$), and 175 mL of 0.2 N H_2SO_4. The solutions were then mixed together outside of the lamps for 10 s before adding to the reactor (containing glass slides with no TiO_2 coating) under the lamps. The contents of the reactor were then rapidly circulated by pump (166 mL/min) by connecting the reactor outlet and inlet with tubing. Ten samples (60 μL) were then collected at regular intervals for 15 min, mixed with 4.94 mL of a ferrozine colorimetric agent solution (0.4 g/L buffered at pH 7 with 0.06 M MOPS), and analyzed by spectrophotometer at λ = 562 nm. Four replicate experiments yielded a photon flux of $9.31(\pm 1.62) \times 10^{-7}$ E/s.

Several procedures were used to characterize the photocatalyst films before and after treatment of micropollutants. Film thickness was measured using profilometry (Sloan Dektak[3]) after etching a cross section out of thin film with a razor blade. Average thickness was determined by analysis of 3 parallel (across same etch) surface scans of 3.5 mm length collected for 3 replicate films. A stylus tracking force of 15 mg was applied for profilometry analysis. X-ray diffraction (XRD) analysis of the immobilized films was conducted using a Panalytic/Philips X'Pert MRD system using Cu Kα radiation, and crystalline phases were determined by comparison

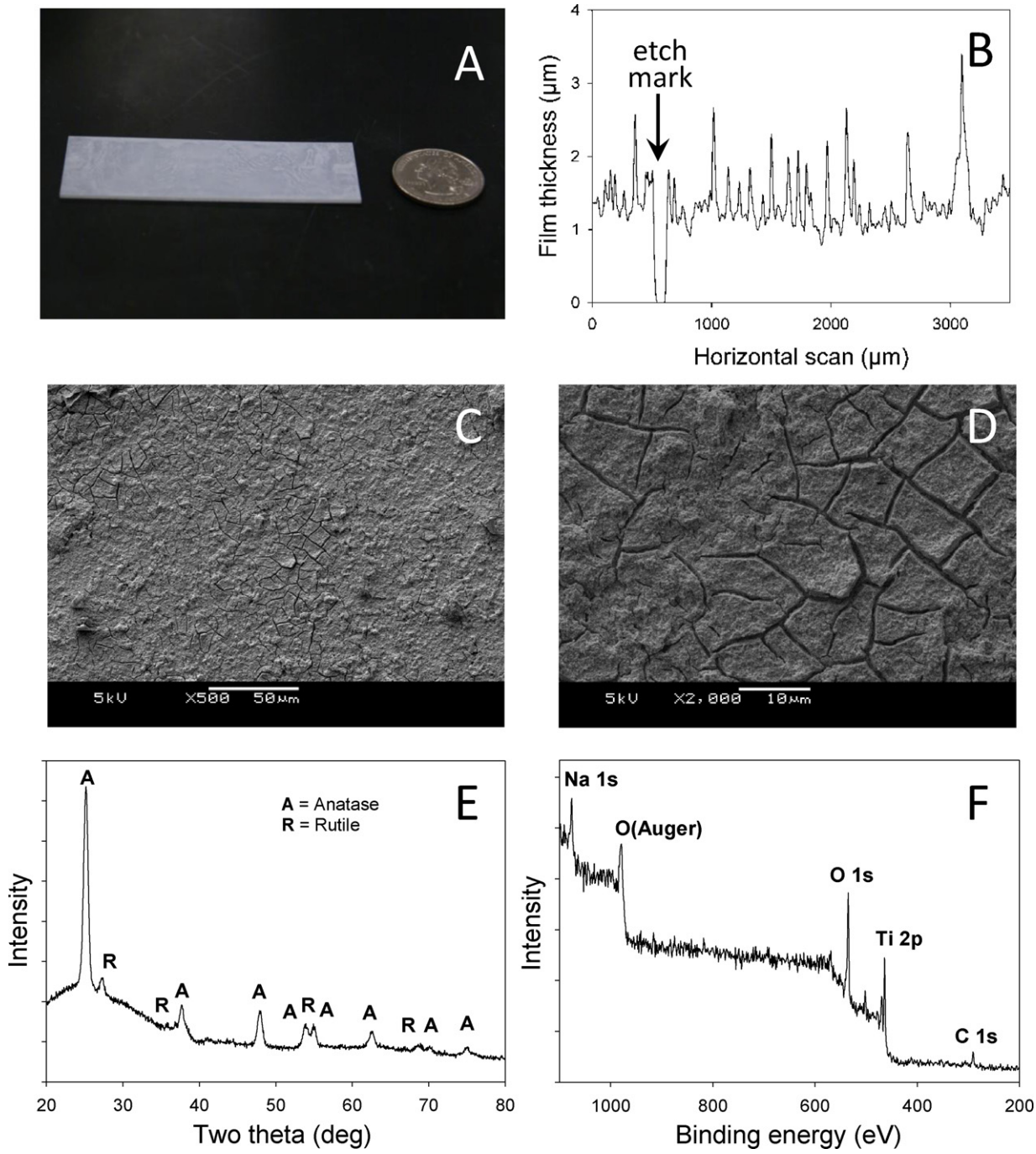

Fig. 3. Characterization of virgin TiO_2 photocatalyst thin films including photograph with comparison to US quarter (A), profilometry (B), representative SEM micrographs at two different magnifications (C and D), X-ray diffractogram (E), and X-ray photoelectron spectra (F).

against the Powder Diffraction File (PDF) database. X-ray photoelectron spectroscopy (XPS) measurements were collected using a Physical Electrons PHI 5400 system. Energy-normalization of the spectra was accomplished by shifting the C 1s peak to 285 eV. Survey data presented in the paper were captured by 5 passes collected over 12 min. Scanning electron microscopy with energy dispersive X-ray spectroscopy (SEM-EDS) was performed using a JEOL JSM-6060LV. Samples were sputter-coated with Au/Pd prior to analysis.

2.5. Batch micropollutant treatment experiments

Micropollutant treatment experiments, both with and without photocatalysts present, were first conducted in the reactor operated in rapid circulating batch mode with laboratory prepared solutions spiked with 50 μg/L of each target micropollutant. The micropollutant-spiked solutions were buffered at pH 8.2 and 10 mM ionic strength (1 mM $NaHCO_3$ + 9 mM NaCl); these conditions will hereafter be referred to as the "buffered electrolyte" matrix. The pH value was selected to match the WWE matrix used in later experiments. $NaHCO_3$ and NaCl were selected as the major pH buffer and electrolyte, respectively, because of their presence in the WWE matrix and their general relevance in natural water matrices; mM levels are typically present in most natural waters, including the WWE. Although HCO_3^- and Cl^- can act as scavengers of $^{\bullet}OH$ [32], little inhibition of photocatalytic processes is reported at the concentrations used in the buffered electrolyte matrix [33,34].

This was confirmed by preliminary tests that showed no significant effects of increasing $NaHCO_3$ concentration to 3 mM or using $NaClO_4$ (non-scavenger of •OH) in place of NaCl. In addition, the focus of studies described here was to assess potential inhibition and deactivation of TiO_2 photocatalysts by processes other than •OH scavenging by background levels of dissolved carbonate ions that will be present in any open reactor system.

For the circulating batch reactions, the reactor contents were first filled with 325 mL of micropollutant-spiked buffered electrolyte solution. Reactor influent and effluent channels were closed and the reactor contents were circulated from the effluent to influent ends at a rate of 166 mL/min. After allowing lamps to warm up for >1 h, experiments were initiated by placing the reactor under the lamps. Aliquots (1 mL) of the reactor solution were then periodically collected for analysis of micropollutant concentrations from the center of the middle lane. Results were used to quantify the relative photocatalytic reactivity of individual micropollutants under baseline solution conditions lacking constituents commonly enriched in wastewater effluent (e.g., effluent organic matter, ammonia). Results from catalyst-free batch reactions were also used to assess the potential importance of UV-A direct photolysis processes for degradation of target micropollutants in the reactor.

Experiments were conducted using initial micropollutant concentrations of 50 μg/L. This value was selected because it was low enough to represent only a small (<1%) fraction of the total dissolved organic carbon (DOC) present when treating natural water matrices like the WWE used here, but high enough to permit quantification of treated solutions (where C_{eff} is only a few μg/L in some cases) by liquid chromatography-tandem mass spectrometry (LC–MS/MS) analysis without matrix interferences or need for pre-concentration by solid phase extraction. Thus, although the spiked concentrations significantly exceeded those typically detected in wastewater effluent (usually <1 μg/L [2]), they were still low enough to be considered only minor solution constituents, and so similar matrix effects were expected. Although future experiments will be needed to confirm that major trends and conclusions drawn from this work remain valid at micropollutant concentrations more typical of wastewater effluent, it is worth noting that preliminary tests showed similar results when initial concentrations were reduced from 50 to 5 μg/L.

2.6. Continuous-flow micropollutant treatment experiments

Continuous-flow micropollutant treatment experiments were conducted to evaluate long-term activity of photocatalysts as well as the effects of treating micropollutants present in WWE containing high levels of effluent organic matter (EfOM) and other inorganic constituents. Experiments were initiated in a similar manner as the batch experiments. After allowing lamps to warm up, treatment experiments were begun by irradiating the reactor initially filled with 325 mL of the desired feed solution spiked with the four target pharmaceutical micropollutants (50 μg/L each). Fresh micropollutant feed solution was then introduced to the influent end of the reactor at the desired flow rate (2.7 mL/min) and effluent was released by flow over the outlet weir. Samples of influent and effluent were then periodically collected for analysis to determine the fraction of each target micropollutant remaining after photocatalytic treatment (C_{eff}/C_{inf}). Flow rates were checked by volumetric analysis of reactor effluent measured for a length of time (>2 h). Effluent samples were collected from a location immediately in front of the effluent weir. Between six and eight effluent samples per operating day were collected. Influent feed reservoir samples were also collected each day. Only one influent sample per operating day was collected because measurements showed values of C_{inf} to be stable.

Table 1
WWE characteristics.

Parameter	Concentration
pH	8.2
Alkalinity	104 mg/L as $CaCO_3$
TDS	427 mg/L
DOC	5.8 mg C/L
Dissolved inorganics[a]	Na (79.8 mg/L), Ca (28.9 mg/L), Mg (21.5 mg/L), K (8.0 mg/L), Si (4.59 mg/L), P (2.84 mg/L), Br (0.18 mg/L), Sr (0.15 mg/L), Fe (0.12 mg/L), Zn (0.06 mg/L), Ba (0.04 mg/L), Al (0.02 mg/L), Mo (0.01 mg/L), Mn (0.01 mg/L), Li (8 μg/L), Cu (6 μg/L), I (6 μg/L), Rb (5 μg/L), Ni (4 μg/L), Cr (3 μg/L), Se (3 μg/L), Cs (3 μg/L), Ti (2 μg/L), V (2 μg/L), As (2 μg/L), B (1 μg/L), Sn (1 μg/L), Pb (1 μg/L), U (1 μg/L)
Dissolved anions[b]	0.96 mM NO_3^-, 2.3 mM SO_4^{2-}, 1.76 mM Cl^-, 0.057 mM PO_4^{3-}
Charge balance[c]	−2.5 mM (26% deficiency of cations)

[a] Measured by ICP-MS.
[b] Measured by IC-CD.
[c] Estimated by $\sum n_i C_i$, where n_i and C_i are the ionic charge and measured molar concentration, respectively, of individual inorganic ions.

Initially, photocatalytic treatment of micropollutants was evaluated in buffered electrolyte matrix. Short-term experiments were conducted to assess the time needed to reach steady-state effluent concentrations and compare the relative reactivity of individual micropollutants with that observed when the reactor was operated in rapid circulating batch mode. Continuous treatment of micropollutants in the buffered electrolyte matrix was then monitored for 7 d to evaluate overall reactor and photocatalyst stability.

Experiments evaluating the effects of WWE on photocatalytic treatment of the target micropollutants were conducted in three stages. Experiments were initiated with the buffered electrolyte matrix as described above, and micropollutant treatment was monitored for 1 d to establish a baseline steady-state treatment level. Then, the influent feed solution was switched to micropollutant-spiked WWE, and treatment of the micropollutants was monitored 4 d. Finally, the influent feed solution was switched back to the buffered electrolyte matrix and monitored for another 2 d to evaluate to what extent catalyst activity returned to pre-WWE treatment levels.

Similar experiments were then conducted to assess whether or not the effluent organic matter or inorganic constituents in the WWE were predominantly responsible for the observed matrix effects. Two approaches were used. First, a continuous-flow micropollutant treatment experiment was conducted using the same WWE matrix that had been pre-treated to reduce the DOC level (WWE matrix equilibrated for 24 h with 4 g/L of GAC before removing GAC particles by filtration; Whatman 2.5 μm circle filter paper). In a second approach, continuous-flow micropollutant treatment was measured in a synthetic "Inorganic WWE mimic" solution prepared by adding to deionized water all the major inorganic components (≥10 μg/L) measured in the actual WWE (Table 1). The original WWE composition was characterized in only a single sample and the estimated charge balance showed a 26% difference between measured values of cationic and anionic inorganic species, indicating some level of collective uncertainty in measured ionic composition. In preparing the "Inorganic WWE mimic" solution, the charge balance was closed by additional Na^+.

2.7. Analytical

LC–MS/MS analysis was used to quantify the four micropollutants (Agilent 1200 Series LC, Agilent LC/MSD Trap XCT Ultra). A Zorbax Eclipse XDB-C18 column (2.1 mm × 50 mm, 3.5 μm particle size) was used as the stationary phase and a gradient mobile phase (0.2 mL/min) was used with two solvents (A: 95% water, 5% acetonitrile, and 0.1% formic acid; B: 5% water, 95% acetonitrile, and 0.1% formic acid). Following injection of filtered samples, solvent B was increased from 0 to 60% over 10 min, then from 60 to 100% over the next 10 min, then decreased back to 0% over the next 0.1 min and held constant for 12 min. Individual micropollutants were quantified by selective ion monitoring mode with the following retention times and ion transitions: IOP (16.7 min, m/z 792 → 573); APAP (17.5 min, m/z 152 → 110); SMX (22.5 min, m/z 254 → 156); CBZ (23.5 min, m/z 237 → 194). Limits of quantification (LOQ) in the WWE were approximately 0.5 μg/L for each micropollutant. Perchlorate was quantified by ion chromatography with conductivity detection (IC-CD; Dionex ICS-2000, 100 μL sample loop, Dionex IonPac AS16 column, 36 mM KOH eluent, 1 mL/min eluent flow rate).

Major water quality parameters for the WWE (pH, alkalinity, TDS) were determined according to *Standard Methods for the Examination of Water and Wastewater* [35]. Major anions were analyzed by IC-CD (Dionex IonPac AS18 column). Metals analysis was conducted by inductively coupled plasma-mass spectrometry (ICP-MS; PerkinElmer Sciex Elen DRCe). DOC was measured using a Shimadzu TOC-VCPH combustion analyzer.

3. Results and discussion

3.1. Catalyst characterization

Fig. 3 summarizes the characterization of the immobilized TiO_2 thin films. SEM analysis of the films (Fig. 3C and D) yielded similar features to those reported by Balasubramanian et al. [36]. The grain size in the porous film was roughly 100–200 nm. We also noted the development of microcracks in the film surface. Agglomerates of TiO_2 on the order of 1–10 μm also formed on the surface of films [37]. EDS analysis (not shown) indicated the presence of Ti, O, C, together with elements presumed to originate from the glass microscope slide support or sol gel components (Si and lesser amounts of P, Cl, Na, and K).

Profilometry analysis (Fig. 3B) indicated an average thickness for the porous TiO_2 films of 1.30(±0.34) μm after 3 dipcoating/heat treatment cycles. This compares with an average primary particle size for Degussa P25 of 30 nm [29]. When using a similar dipcoating procedure, Balasubramanian et al. achieved a thickness of 110 μm from 3 coating/heat treatment cycles on a stainless steel support [36], approximately 85 times the thickness observed here.

Quantitative analysis of the X-ray diffraction data (Fig. 3E) indicated that the film contained a crystalline component composed of 78% anatase and 22% rutile. This is consistent with previous reports of Degussa P25 [36]. The crystallite size of anatase and rutile were 196 Å and 347 Å, respectively. These results compare reasonably well with that reported by Balasubramanian et al. [36], with major differences being attributed to the support substrate (glass versus stainless steel).

Prominent peaks observed with XPS analysis (Fig. 3F) included Ti 2p, C 1s, and O 1s and Auger peaks, consistent with the elements observed with SEM-EDS. The double peak of Ti 2p was expected for TiO_2. The C 1s comes from the incomplete pyrolysis of diethanolamine and isopropanol during heat treatment of the immobilized sol [37]. The observed Na 1s peak may result from two potential sources. Spectra collected for the Degussa P25 TiO_2 nanoparticles mixed into the TiO_2 sol–gel also exhibited a weak Na 1s peak, suggesting it may be a source. Alternatively, a number of studies have reported sodium migration from glass support slides through immobilized TiO_2 thin films during film calcination [38,39], and others have reported migration of metals from stainless steel supports through TiO_2 films thicker than those used in this study during calcination [37].

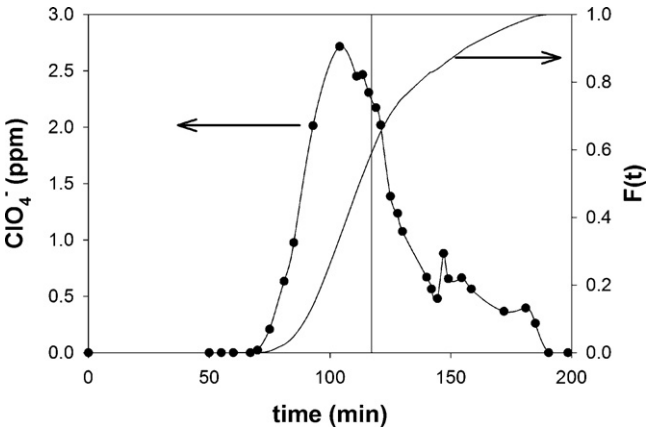

Fig. 4. Reactor outlet concentration of ClO_4^- tracer and cumulative tracer function $F(t)$; vertical line indicates measured mean residence time (τ = 117 min).

3.2. Reactor characteristics

Conservative tracer and batch treatment experiments were first conducted to separately characterize the hydraulic and photocatalytic properties of the reactor system. Fig. 4 shows the result of a tracer experiment. Effluent concentrations of perchlorate began to be detected ~70 min after pulse input of $NaClO_4$, then increased to a peak value at ~100 min before slowly decreasing to non-detectable levels by ~190 min. Calculation of the mean residence time yielded a value of 117 min [40], which agrees with the theoretical residence time of 120 min (V/Q = 325 mL/2.7 mL/min = 120 min). Analysis of tracer data also revealed a Péclet number of 44 and longitudinal dispersion coefficient (D_L) of 1.2×10^{-5} m^2 s^{-1}. Although the transverse dispersion coefficient (D_T) is not known from the tracer data, solute mixing across the depth of the plugflow reactor channel will be controlled by dispersion and will be fast compared to the characteristic timescale of the observed reactions discussed below even if D_T is only a small fraction of D_L.

Fig. 5 shows timecourses for photocatalytic degradation of the four target micropollutants in replicate experiments measured in buffered electrolyte where the reactor was operated in rapid circulating batch mode. Although heterogeneous catalytic processes are complex multistep interfacial processes, timecourse data was fit with a pseudo-first-order rate model to obtain a simple measure of each micropollutant's observed treatment efficiency in the reactor setup; this value could then be compared with other reactor operating conditions and solution matrices. Model fits yielded observed rate constants (k_{obs}, ±95% CI) that varied from IOP (0.43 ± 0.07 h^{-1}) < CBZ (0.51 ± 0.05 h^{-1}) < SMX (0.58 ± 0.06 h^{-1}) < APAP (0.94 ± 0.14 h^{-1}). These k_{obs} values were then expected to be the maximum degradation rate constants at the selected solution conditions and water depth overlying the photocatalyst films. As mentioned in Section 2.5, although HCO_3^- and Cl^- can act as scavengers of •OH at elevated concentrations [32], tests indicated minimal effect of the ions on micropollutant treatment efficiencies at concentrations present in the buffered electrolyte matrix. A catalyst-free photolysis control experiment was also conducted to assess the potential relevance of direct photolysis reactions. Minimal degradation of the target

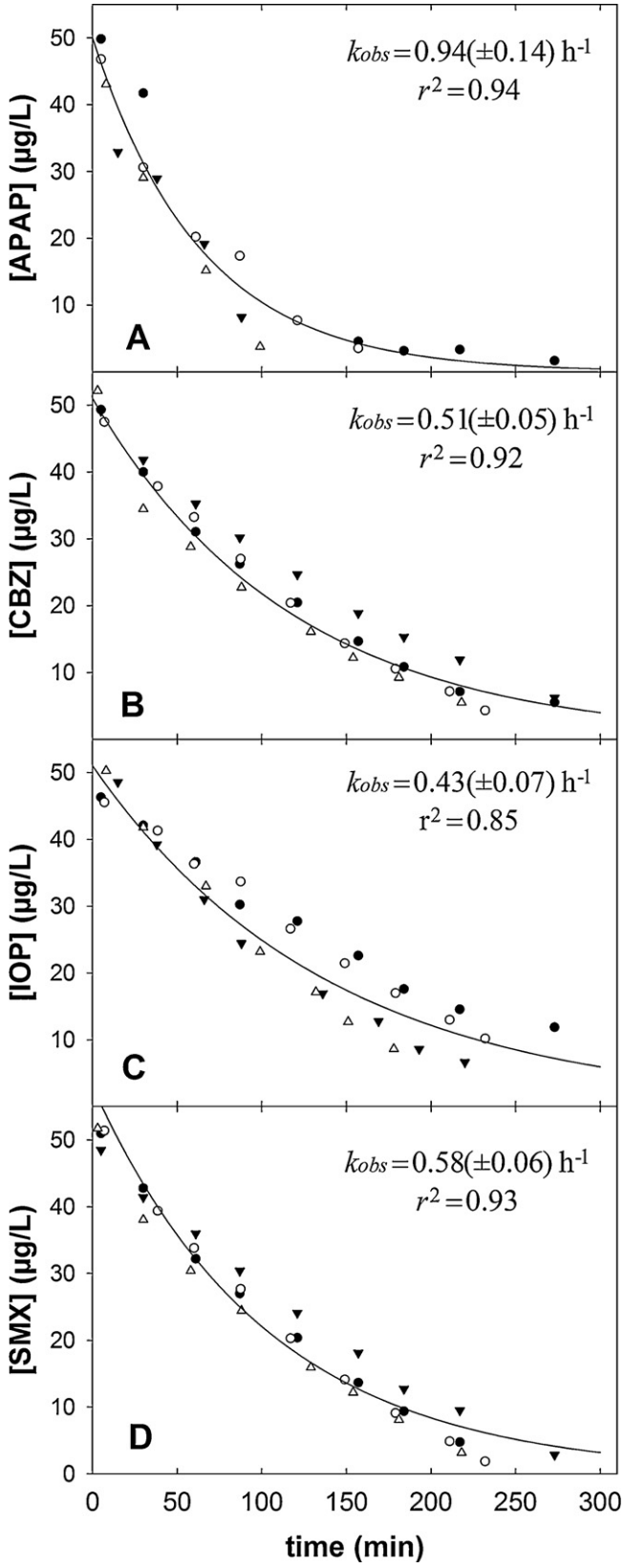

Fig. 5. Circulating batch photocatalytic degradation kinetics of the four micropollutants in the buffered electrolyte matrix. Individual replicate experiments are represented by different symbols. Fit-derived k_{obs} values and associated uncertainties (95% CI) derived from regression of the combined data set for each compound.

micropollutants was observed in the circulating reactor within 6 h ($k_{obs} < 0.02\ h^{-1}$), indicating negligible contribution to the micropollutant losses observed during TiO_2 photocatalytic treatment.

Here, three dip coating/heat treatment cycles were used to prepare the catalyst thin films because initial tests indicated no significant improvement in photocatalytic activity with application of coatings. Although not the subject of this study, previous work suggests that the apparent rate constants for micropollutant treatment can be further improved by modification of several variables found to affect the activity of supported thin film TiO_2 photocatalysts, including number of repeated film applications, sol–gel composition, catalyst additives, and support type [36].

No comparable studies using thin-film TiO_2 photocatalysts for degrading these micropollutants are available for comparing reactivity trends. However, relative reactivity trends of the same micropollutants have been noted in studies conducted in TiO_2 suspensions. Miranda-García et al. [28] observed similar photocatalytic degradation rates for SMX and CBZ (differ by <10%) in UV-irradiated suspensions of TiO_2, in agreement with the trend observed here. Like here, Doll and Frimmel [12] also observed similar reactivities for CBZ and iomeprol (structurally related to iopromide) in batch suspensions of P25 TiO_2 (rates differ by ~16%). Finally, Klamerth et al. [19] reported slower photocatalytic degradation of SMX compared to APAP.

Reactivity trends among the four compounds can also be compared with the rate constants for homogeneous reactions with •OH. This comparison reveals no obvious relationship between the reactivity trends in photocatalytic systems and the trend in reported homogeneous second-order rate constants with •OH: APAP ($2.2 \pm 0.02 \times 10^9\ M^{-1}\ s^{-1}$) < IOP ($3.3 \pm 0.6 \times 10^9\ M^{-1}\ s^{-1}$) < SMX ($5.5 \pm 0.7 \times 10^9\ M^{-1}\ s^{-1}$) < CBZ ($8.8 \pm 1.2 \times 10^9\ M^{-1}\ s^{-1}$) [6,41]. However, it is difficult to draw mechanistic conclusions (e.g., identification of controlling reactive surface species) from this comparison because photocatalysis is a complex interfacial process and the observed rate constants for photocatalytic treatment of micropollutants include contributions from adsorptive interactions in addition to surface redox reactions with photo-generated reactive species (i.e., Langmuir–Hinshelwood kinetic models) [16].

3.3. Continuous-flow treatment: steady-state operation and reactor stability

Continuous-flow experiments (i.e., single pass treatment of reactor influent) were first conducted in the same buffered electrolyte matrix used for batch experiments. Initially, the reactor was filled with solution containing 50 µg/L of each micropollutant. Once flow was initiated and photocatalysts were exposed to UV lamps, effluent concentrations of the micropollutants began to decrease until steady-state levels were approached after ~4 h, as shown for IOP in Fig. 6. Subsequently, monitoring of reactor effluent was begun after allowing ~12 h of continuous treatment to ensure that steady-state conditions had been reached.

Previous tests in batch systems demonstrated minimal degradation of micropollutants in catalyst-free solutions irradiated for 6 h, and continuous-flow dark control experiments indicated no detectable loss of micropollutants in the absence of UV-A irradiation (e.g., by adsorption to the catalyst films) over a 6 h period. Thus, it was concluded that UV-TiO_2 photocatalytic processes were responsible for the decreased micropollutant concentrations observed in the reactor effluent.

To evaluate long-term catalyst and reactor stability in the absence of complicating solution conditions, micropollutant treatment in the buffered electrolyte matrix was monitored continuously for 7 d. Fig. 7 shows the treatment level achieved for each micropollutant over the course of the experiment. Overall, the level of treatment for all four target micropollutants was stable over the

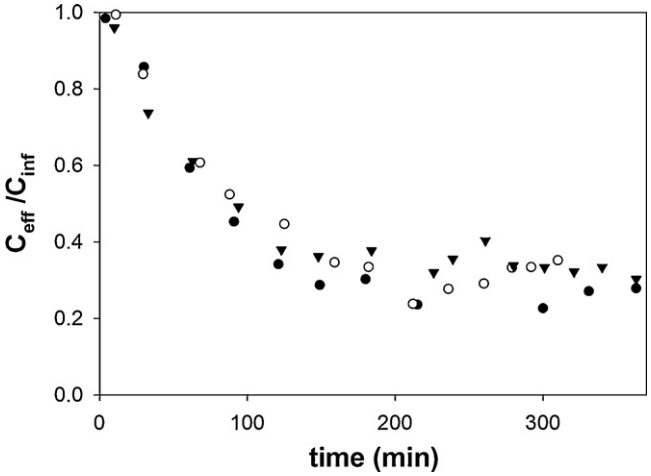

Fig. 6. Initial continuous-flow reactor data for photocatalytic treatment of IOP establishing a steady-state level of treatment; different symbols represent individual replicate experiments.

entire period monitored, with no clear trends indicating decreases or increases in reactor performance due to extended use of photocatalysts or lamps. Tests also show that flow rates remained stable over the monitored period. Mean levels of treatment ranged from to 62% removal of IOP and CBZ to 84% removal of APAP. Profilometry analysis of catalyst films showed no effect of catalyst use for 7 d on the film thickness or roughness, indicating physical stability of the films under hydraulic and irradiation conditions used in this study.

Fig. 8 shows the k_{obs} values derived from the continuous-flow treatment experiments (Fig. 7) with values obtained from the circulating batch experiments (Fig. 5). The former were calculated from the measured steady-state effluent and influent concentrations by assuming plug flow with a mean residence time (τ) of 117 min, determined from tracer studies (Fig. 4):

$$k_{obs} = \frac{-\ln(C_{eff}/C_{inf})}{\tau} \quad (1)$$

In general, the 7-d averaged k_{obs} values (±95% CI) determined under continuous-flow conditions ($0.49 \pm 0.03\ h^{-1}$ for IOP; $0.97 \pm 0.10\ h^{-1}$ for APAP; $0.79 \pm 0.06\ h^{-1}$ for SMX, $0.50 \pm 0.04\ h^{-1}$ for CBZ) agreed closely with those measured in circulating batch mode; only the mean value measured for SMX was found to be significantly different, being 36% higher than the mean value measured in circulating batch mode. The general agreement between measurements from the two operational modes confirms the validity of using continuous-flow treatment data and a plug flow model to assess the activity of photocatalysts with different micropollutants. The close match between values measured under the low flow-rate continuous-flow conditions (2.7 mL/min) and those measured in rapid circulating batch mode with flow rates that were nearly two orders-of-magnitude higher (166 mL/min) also demonstrate that the observed reaction rates are not limited by mass transfer through a fluid boundary next to the catalyst film surface. It also follows that the continuous-flow treatment experiments can be used to quantify the effects of non-target water constituents on the chemical reaction properties of the immobilized catalyst films.

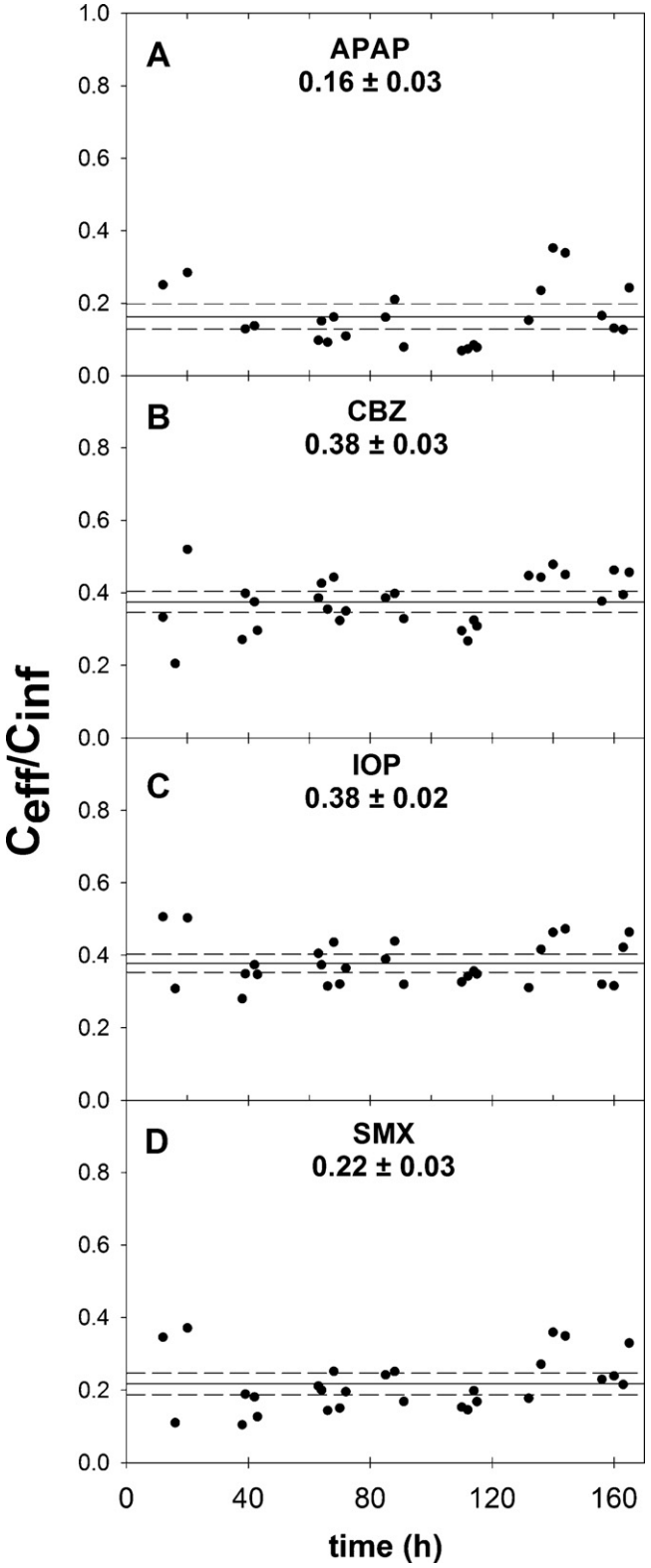

Fig. 7. Continuous treatment of micropollutants for 7 d in buffered electrolyte matrix. Mean and 95% confidence intervals indicated with solid and dashed lines, respectively.

3.4. Photocatalytic treatment of micropollutants in WWE

Major characteristics of the WWE are shown in Table 1. Of particular importance, the WWE contained a significant DOC level (5.8 mg C/L), so addition of the four micropollutants collectively increased DOC by <2% (107 μg/L) and did not affect bulk properties of the matrix. The WWE also contained a number of inorganic constituents, and the measured pH and alkalinity levels were suggestive of a similar level of dissolved bicarbonate as the laboratory-prepared buffered electrolyte solutions.

Fig. 9 shows the results of representative continuous-flow treatment experiments for each of the target micropollutants. The

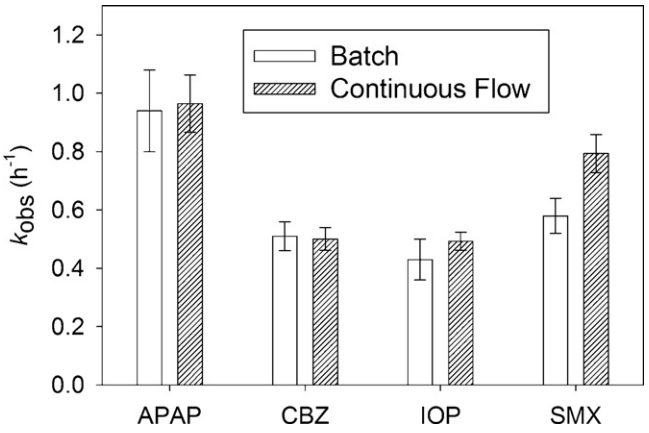

Fig. 8. Comparison of k_{obs} values for the target micropollutants determined in circulating batch experiments (Fig. 5) and 7-d continuous-flow experiments (Fig. 7). Uncertainty = 95% CI.

vertical dashed lines separate each of the three treatment regimes. After establishing steady-state levels of micropollutant treatment in the buffered electrolyte matrix over the first day, the influent was switched to the WWE matrix for the next 4 d, followed by a return to the buffered electrolyte matrix for the final 2 d. For all four target micropollutants, the efficiency of photocatalytic treatment was reduced upon switching the reactor feed to the WWE matrix, but the extent of the decrease varied among the micropollutants (APAP = 40% decrease; CBZ = 60%; IOP = 78%; SMX = 54%). The largest effect occurred for IOP, where the mean level of treatment decreased from 62% removal in buffered electrolyte to just 19% removal from WWE (a 78% drop in treatment efficiency). In contrast, comparable matrix changes only decreased the mean level of APAP removal from 84% to 68% (a 40% drop in treatment efficiency). IOP is the most recalcitrant of the tested pharmaceuticals, reacting only with the strongest chemical oxidants (e.g., •OH [42]), whereas the others contain moieties that are oxidized by a wider range of chemical oxidants (e.g., phenolic and aniline groups can be oxidized by $CO_3^{\bullet -}$, $O_2^{\bullet -}$ [43]). Therefore, these results are consistent with WWE matrix constituents scavenging photocatalyst-produced •OH. It is also worth noting that little change in the overall DOC level (<5%) in WWE was observed during photocatalytic treatment, consistent with expectations that mineralization of organics only occurs upon extended exposure to AOPs.

Somewhat surprisingly, treatment efficiencies for most of the pharmaceuticals largely returned to the pre-WWE levels when the feed solution was switched back to buffered electrolyte after 4 d of continuously treating the micropollutants in WWE. Fig. 10 compares the mean rate constants observed for each of the three treatment regimes. The rate constants were reduced in the WWE matrix to varying degrees as expected from the effluent monitoring data in Fig. 9, but much of the decreases were erased upon switching back to buffered electrolyte, suggesting that a large fraction of the observed decrease in treatment efficiency in WWE was readily reversible over the timescale that catalysts were exposed to the WWE matrix. This suggests that many constituents in the WWE were acting to competitively inhibit photocatalyst reactions with the target micropollutants (e.g., by scavenging of photocatalyst-generated •OH or reversibly adsorbing to reaction sites), but were not acting to irreversibly poison or deactivate the photocatalyst materials.

The observed decreases in treatment efficiency of individual micropollutants in WWE can result from reversible inhibition of photocatalyst reactions by non-target water constituents as well as processes that irreversibly deactivate the photocatalyst (may still be reversible, but not without harsher intervention).

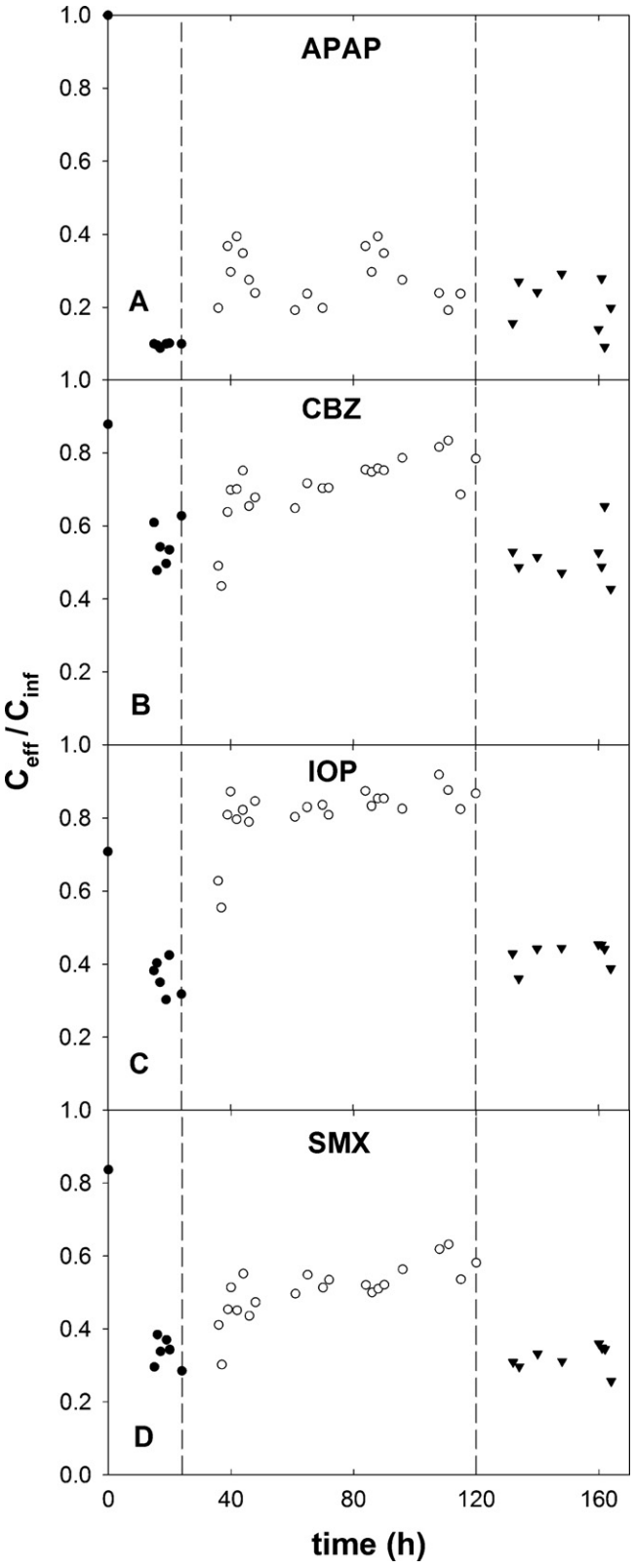

Fig. 9. Representative experiment showing treatment of the four target micropollutants in the buffered electrolyte matrix (●), WWE (○), and returning to buffered electrolyte matrix (▼). Vertical dashed lines indicate time of influent switching.

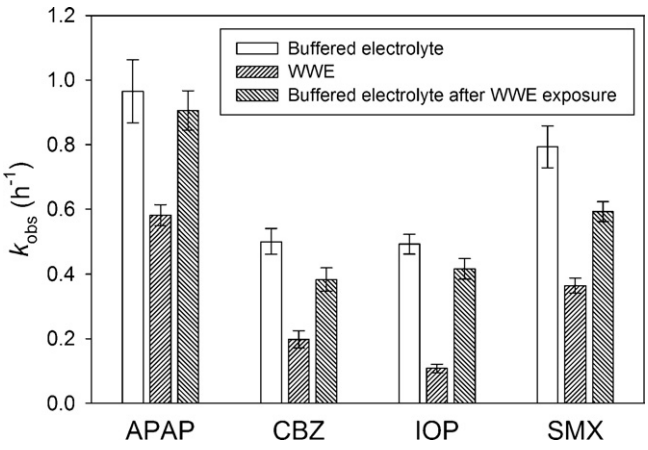

Fig. 10. Mean k_{obs} values for each micropollutant before, during, and after exposure to WWE. Uncertainty = 95% CI.

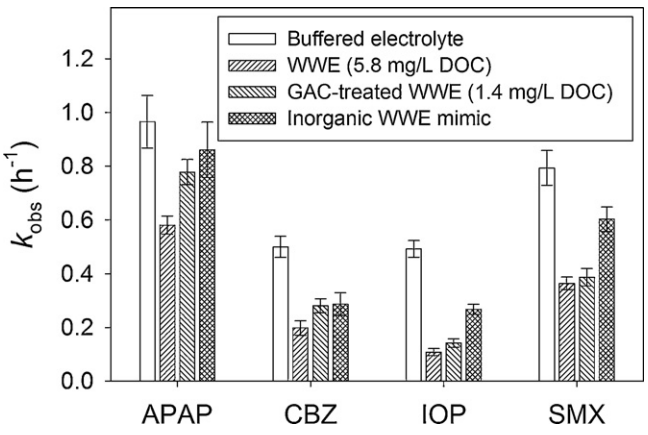

Fig. 11. Comparison of observed reaction rate constants in micropollutant-spiked buffered solution, WWE, GAC-treated WWE, and in a laboratory "mimic" solution of the inorganic components measured in the WWE matrix. Uncertainty = 95% CI.

The easily reversible "catalyst inhibition" versus more irreversible "catalyst deactivation" can operationally be defined as the percentage decreases in k_{obs} measured when switching from buffered electrolyte to WWE that were recovered versus not recovered, respectively, upon switching back to the buffered electrolyte matrix. Using these operational definitions, the majority of the reductions in treatment efficiency observed in the WWE matrix were recoverable and thus attributable to processes that reversibly inhibit photocatalyst reactions with the target contaminants. Still, the apparent extent of catalyst deactivation after 4 d of continuous treatment in WWE was significant for some of the target micropollutants (6% deactivation for APAP treatment; 16% for IOP; 24% for CBZ; 25% for SMX), indicating that non-target constituents in the WWE also contributed to photocatalyst deactivation. Inhibition can result from reversible blocking of surface reaction sites or scavenging of photocatalyst-produced radicals by non-target water constituents. Deactivation may result from accumulation of selected constituents on catalyst surfaces that suppress the activity of catalysts. Still, the efficiency of micropollutant treatment in the WWE matrix appeared to remain stable for the 4 d in the WWE, suggesting that the extent of deactivation was not changing significantly on the timescale of experiments conducted here. Thus, it is unclear whether the extent of deactivation will increase with more extended exposures to the WWE matrix, and longer term continuous treatment experiments are needed to address this question. In addition, studies are needed to test potential pretreatment and photocatalyst regeneration strategies for extending catalyst longevity.

3.5. Identifying catalyst-inhibiting and deactivating constituents in WWE

Although the WWE matrix contains a large number of constituents that might influence photocatalytic reactions with the target micropollutants, previous studies suggest that the effluent organic matter may be playing a prominent role in the observed inhibition. Dissolved organic matter can affect photocatalytic treatment processes in several ways [12]: (1) act as competitive scavengers of •OH to reduce the effective concentration available for reacting with target micropollutants, (2) competitively inhibit adsorption of the target micropollutants, thereby reducing interactions with adsorbed •OH, and (3) absorb incident photons, reducing the available UV-A photon flux for TiO_2 excitation (i.e., screening). That said, results of continuous-flow treatment experiments showed only a small effect of reducing the DOC level in the WWE matrix from 5.8 mg C/L to 1.4 mg C/L (by GAC treatment). Despite the 75% reduction in DOC, the mean k_{obs} values for 2 of the 4 micropollutants measured in WWE were little affected (Fig. 11). This finding suggests that either EfOM is not the only major constituent responsible for inhibition/deactivation of photocatalysts in WWE or that the EfOM fraction removed by GAC pretreatment was less catalyst inhibiting/deactivating than the fraction that was not removed. It would not be surprising that the EfOM constituents that are most surface reactive with a polar metal oxide like TiO_2 would be less amenable to adsorption by nonpolar GAC. However, further research is needed before making such conclusions.

The role of non-DOM constituents in WWE was evaluated separately by examining micropollutant treatment in a laboratory "mimic" solution of the major inorganic components of the WWE described in Table 1. Results of these experiments showed that micropollutant treatment was inhibited/deactivated somewhat relative to buffered electrolyte, but to a lesser extent than in the WWE that also contains EfOM. Several of the inorganic species in the WWE have been shown to inhibit or deactivate photocatalytic processes, including dissolved carbonate and phosphate species, Cl^-, NO_3^-, SO_4^{2-}, and metal ions like Fe and Mn [33,34]. Thus, these results suggest that both organic and inorganic constituents in the WWE are contributing to the observed inhibition/deactivation of photocatalysts, and further studies will be needed to identify those individual constituents that inhibit photocatalysts and to evaluate the merits of pretreating WWE to selectively remove these constituents prior to photocatalyst treatment.

The above results provide an indication of the expected range of effects of WWE matrix constituents on photocatalytic treatment of trace micropollutants. Efforts were made to employ low concentrations of the target micropollutants in the reactor feed (50 μg/L; adding <1% new DOC to the WWE matrix) to ensure minimal effects on bulk matrix properties, and consequently replicate the effects that matrix constituents will have on treatment of the monitored micropollutants. Although care should be taken when comparing homogeneous reactions with heterogeneous processes like TiO_2 photocatalysis, comparison of previously reported homogeneous second-order rate constants for •OH reactions with the target micropollutants [6,41] and matrix components (dissolved organic carbon [44] and dissolved carbonate species [45]) does suggest that similar matrix radical scavenging effects will be observed at lower initial micropollutant concentrations more relevant to WWE matrices (e.g., <1 μg/L; < 0.02% of DOC in WWE). For example, the ratio of •OH scavenging of the solution in the absence versus presence of the amended target micropollutants can be estimated

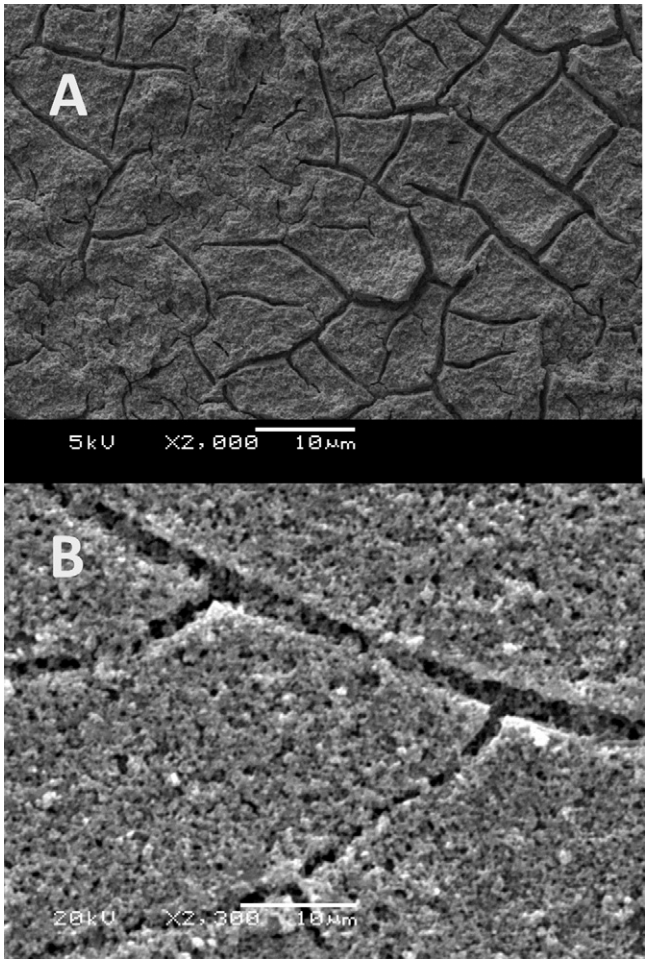

Fig. 12. Scanning electron micrograph of (A) unexposed TiO_2 film, (B) TiO_2 film following 4 d of exposure to WWE matrix when treating micropollutants.

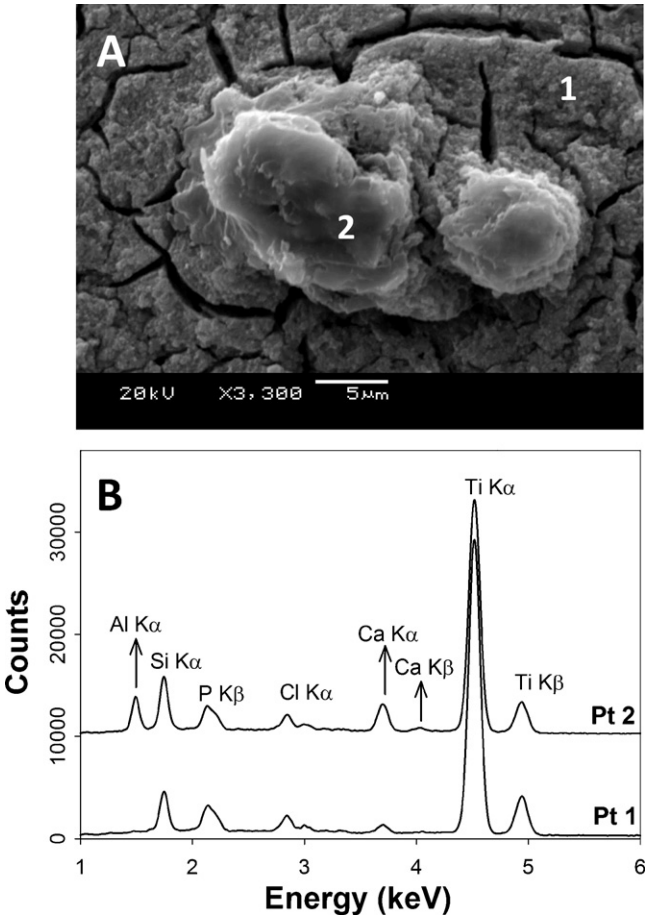

Fig. 13. (A) Scanning electron micrograph closeup and (B) energy dispersive X-ray spectra of the TiO_2 thin film (Pt 1) and a representative surface precipitate (Pt 2) that formed during the continuous-flow treatment experiment conducted in WWE.

by the following expression:

$$R_{OH} = \frac{(k_{DOC}C_{DOC} + k_{HCO_3^-}C_{HCO_3^-} + k_{CO_3^{2-}}C_{CO_3^{2-}})}{(k_{DOC}C_{DOC} + k_{HCO_3^-}C_{HCO_3^-} + k_{CO_3^{2-}}C_{CO_3^{2-}}) + \sum_{MP} k_{MP}C_{MP}} \quad (2)$$

where C_i and k_i represent the molar concentration of matrix component or micropollutant "i" and its second-order rate constant reaction with •OH reaction ($M^{-1}\,s^{-1}$). Values of R_{OH} approaching unity indicate minimal effects of amended micropollutants on overall •OH scavenging by the solution. For the measured DOC and alkalinity levels in the WWE (Table 1), the calculated values of R_{OH} only decreases from 1.00 to 0.98 when the initial concentration of the four target micropollutants increases from 0 to 50 μg/L, indicating only a 2% increase in total •OH scavenging by the micropollutant-amended WWE matrix. Only when initial micropollutant concentrations approach 1 mg/L is the predicted •OH scavenging significantly perturbed. These calculations support the suggestion that the decreases in micropollutant treatment in WWE observed here are reflective of the decreases that can be expected when treating more environmentally relevant concentrations of the target micropollutants. Still, future work will be needed to confirm this because of the added complexity of the heterogeneous photocatalytic reaction system.

3.6. Catalyst properties post-treatment

TiO_2 films were also re-characterized following exposure to the WWE matrix under treatment conditions for several days. No large changes in the bulk crystal structure or surface chemistry of the films were noted from XRD and XPS analysis, respectively. Visually, a slight brown discoloration developed on the WWE-exposed films. Profilometry analysis exhibited a slight increase in film thickness (1.84 ± 0.61 μm), but the difference was not statistically significant. SEM analysis showed that microcracks that were clearly visible in the virgin films (Fig. 3C and D) were partially filled in following exposure to WWE, and other debris began to appear on the surface of films (Fig. 12B). EDS analysis indicated most of the surface debris was TiO_2, suggesting some minor matrix-promoted deterioration of the film occurred. Markedly less deterioration was evident in TiO_2 thin films following continuous treatment of the buffered electrolyte matrix for 7 d. There was also a sparse amount of small precipitates (1–10 μm) which EDS analysis indicates were enriched in Al and Ca (Fig. 13).

4. Conclusions

In this contribution, we demonstrated a new laboratory benchtop continuous-flow TiO_2 photocatalytic reactor that will be useful for studying critical factors and mechanisms affecting the activity, inhibition, and deactivation of immobilized photocatalysts by non-target water constituents present in diverse matrices that are relevant to the water treatment industry. Through a combination of

tracer studies, circulating batch, and continuous-flow experiments, the reactor and photocatalysis behavior were stable and could be described using a plug flow reactor model. Photocatalytic degradation rates of micropollutants decreased in WWE due to the presence of both organic and inorganic non-target constituents. Still, significant degradation of most of the target micropollutants was sustained for 4 d of continuous treatment in the WWE matrix and the degree of photocatalyst deactivation over this time period was not severe. These findings suggest that longer term studies (e.g., weeks, months) are needed to gain a better understanding of the factors controlling catalyst activity and longevity. In addition, studies are needed to identify the specific constituents responsible for photocatalyst inhibition/deactivation and assess the feasibility of pretreatment and regenerative strategies for increasing removal of the target micropollutants and extending photocatalyst longevity.

Acknowledgments

This work was supported by a National Science Foundation CAREER Award to T. Strathmann (CBET 07-46453) and the Global Collaborative Research Office of King Abdullah University of Science and Technology (KAUST) through the Collaborative Research on Sustainable Water Development and Engineering Partnership. Materials characterization was carried out in part in the Frederick Seitz Materials Research Laboratory Central Facilities, University of Illinois. Zachary Sasnow, Rick Haasch, Charles Werth, and Laura Asmuth (UIUC) are acknowledged for assistance with experimental work and helpful discussions. The manuscript also benefitted from feedback provided by anonymous reviewers.

References

[1] R.L. Oulton, T. Kohn, D.M. Cwiertny, Journal of Environmental Monitoring 12 (2010) 1956.
[2] T.A. Ternes, Water Research 32 (1998) 3245.
[3] C.G. Daughton, T.A. Ternes, Environmental Health Perspectives 107 (1999) 907.
[4] D.L. Sedlak, J.L. Gray, K.E. Pinkston, Environmental Science and Technology 34 (2000) 508A.
[5] C. Zwiener, F.H. Frimmel, Water Research 34 (2000) 1881.
[6] M.M. Huber, S. Canonica, G.-Y. Park, U. von Gunten, Environmental Science and Technology 37 (2003) 1016.
[7] W.R. Haag, C.C.D. Yao, Environmental Science and Technology 26 (1992) 1005.
[8] B. Ning, N.J.D. Graham, Journal of Environment Engineering 134 (2008) 944.
[9] G. Anquandah, M.B. Ray, A.K. Ray, A.J. Al-Abduly, V.K. Sharma, Environmental Technology 32 (2011) 261.
[10] W. Kalsch, Science of the Total Environment 225 (1999) 143.
[11] P. Calza, C. Medana, M. Pazzi, C. Baiocchi, E. Pelizzetti, Applied Catalysis B: Environmental 53 (2004) 63.
[12] T.E. Doll, F.H. Frimmel, Water Research 9 (2005) 403.
[13] Y. Ohko, K.-I. Iuchi, C. Niwa, T. Tatsuma, T. Nakashima, T. Iguchi, Y. Kubota, A. Fujishima, Environmental Science and Technology 36 (2002) 4175.
[14] S. Valencia, J.M. Marín, G. Restrepo, The Open Materials Science Journal 4 (2010) 9.
[15] T.E. Doll, F.H. Frimmel, Catalysis Today 101 (2005) 195.
[16] M.R. Hoffmann, S.T. Martin, W. Choi, D.W. Bahnemann, Chemical Reviews 95 (1995) 69.
[17] Y. Zhang, J.C. Crittenden, D.W. Hand, D.L. Perram, Environmental Science and Technology 28 (1994) 435.
[18] D. Mitoraj, H. Kisch, Angewandte Chemie International Edition 47 (2008) 9975.
[19] N. Klamerth, N. Miranda, S. Malato, A. Agüera, A.R. Fernández-Alba, M.I. Maldonado, J.M. Coronado, Catalysis Today 144 (2009) 124.
[20] L. Rizzo, S. Meric, M. Guida, D. Kassinos, V. Belgiorno, Water Research 43 (2009) 4070.
[21] T.E. Doll, F.H. Frimmel, Water Research 38 (2004) 955.
[22] J. Choina, H. Duwensee, G.-U. Flechsig, H. Kosslich, A.W. Morawski, V.A. Tuan, A. Schulz, Central European Journal of Chemistry 8 (2010) 1288.
[23] C. Lin, K.-S. Lin, Chemosphere 66 (2007) 1872.
[24] T. Papadam, N.P. Xekoukoulotakis, I. Poulios, D. Mantzavinos, Journal of Photochemistry and Photobiology A: Chemistry 186 (2007) 308.
[25] E. Hapeshi, A. Achilleos, M.I. Vasquez, C. Michael, N.P. Xekoukoulotakis, D. Mantzavinos, D. Kassinos, Water Research 44 (2010) 1737.
[26] M.N. Chong, B. Jin, G. Laera, C.P. Saint, Chemical Engineering Journal 174 (2011) 595.
[27] L. Hu, P.M. Flanders, P.L. Miller, T.J. Strathmann, Water Research 41 (2007) 2612.
[28] N. Miranda-García, S. Suárez, B. Sánchez, J.M. Coronado, S. Malato, M.I. Maldonado, Applied Catalysis B: Environmental 103 (2011) 294.
[29] G.V. Nano, T.J. Strathmann, Journal of Colloid and Interface Science 321 (2008) 350.
[30] G. Balasubramanian, D. Dionysiou, M. Suidan, Y. Subramanian, I. Baudin, J. Laine, Journal of Materials Science 38 (2003) 823.
[31] C.G. Hatchard, C.A. Parker, Proceedings of the Royal Society of London, Series A, Mathematical and Physical Sciences 235 (1956) 518.
[32] G.V. Buxton, C.L. Greenstock, W.P. Helman, A.B. Ross, Journal of Physical and Chemical Reference Data 17 (1988) 513.
[33] R.A. Burns, J.C. Crittenden, D.W. Hand, V.H. Selzer, L.L. Sutter, S.R. Salman, Journal of Environment Engineering 125 (1999) 77.
[34] D.C. Schmelling, K.A. Gray, P.V. Kamat, Water Research 31 (1997) 1439.
[35] A.D. Eaton, M.A.H. Franson, A.W.W. Association, W.E. Federation, Standard Methods for the Examination of Water & Wastewater, American Public Health Association, 2005.
[36] G. Balasubramanian, D.D. Dionysiou, M.T. Suidan, I. Baudin, J.-M. Laine, Applied Catalysis B: Environmental 47 (2004) 73.
[37] Y. Chen, D.D. Dionysiou, Applied Catalysis B: Environmental 62 (2006) 255.
[38] J. Yu, X. Zhao, Materials Research Bulletin 35 (2000) 1293.
[39] H. Yu, J. Yu, B. Cheng, Catalysis Communications 7 (2006) 1000.
[40] M.M. Clark, Transport Modeling for Environmental Engineers and Scientists, Wiley-Interscience, 2009.
[41] R. Andreozzi, V. Caprio, R. Marotta, D. Vogna, Water Research 37 (2003) 993.
[42] M.M. Huber, S. Canonica, G.-Y. Park, U. Von Gunten, Environmental Science and Technology 37 (2003) 1016.
[43] S. Canonica, T. Kohn, M. Mac, F.J. Real, J. Wirz, U. Von Gunten, Environmental Science and Technology 39 (2005) 9182.
[44] P. Westerhoff, G. Aiken, G. Amy, J. Debroux, Water Research 33 (1999) 2265.
[45] R.A. Larson, R.G. Zepp, Environmental Toxicology and Chemistry 7 (1988) 265–274.